RESEARCH ARTICLE

Preparation and biocidal properties of MoS_2/rGO nanocomposites

Jingyan Wang*, Deqiu Zhang

School of Civil Engineering, Harbin University, Harbin, Heilongjiang, China.

Received: February 10, 2025; **accepted:** May 21, 2025.

Given the escalating global crisis of drug-resistant bacteria, the effectiveness of conventional antibiotics is steadily diminishing, necessitating the urgent development of novel and potent antibacterial materials. This research applied an optimized Hummers method to prepare graphene oxide followed by using microwave-assisted hydrothermal method to vertically grow molybdenum disulfide nanosheets on the surface of reduced graphene oxide, forming a molybdenum disulfide/reduced graphene oxide vertical heterojunction. The structure and properties of the new metal nanomaterial were analyzed through material characterization and analysis techniques. Meanwhile, *in vitro* and *in vivo* sterilization experiments were conducted to evaluate the antibacterial performance and biosafety of the materials. The results of the *in vitro* sterilization experiment showed that the nanocomposite material prepared in the study had sterilization effects on both Gram negative and positive bacteria. The survival rates of Gram negative and positive bacteria after combined treatment with nanocomposite materials were about 10% and 12%, respectively, while the capture efficiencies of bacteria were about 82.3% and 80.3%, respectively. The results of the *in vivo* sterilization experiment showed that the concentration of white blood cells in the wounds of mice injected with nanocomposite materials and H_2O_2 was maintained at around 3.5K/μL. The results indicated that the nanocomposite material prepared in the study had good sterilization and no significant *in vivo* toxicity. A metal nanocomposite material with efficient antibacterial properties was successfully prepared through this research, which provided not only the new ideas and methods for developing new antibacterial materials, but also the strong technical support for solving the problem of drug-resistant bacterial infections.

Keywords: drug-resistant bacteria; antibiotic; metal nanomaterials; molybdenum disulfide nanosheets; graphene; chemical synthesis.

***Corresponding author:** Jingyan Wang, School of Civil Engineering, Harbin University, Harbin 150000, Heilongjiang, China. Email: wangjingyan202208@126.com.

Introduction

Against the backdrop of increasingly severe global public health challenges, bacterial infections and the various diseases they cause continue to pose a major threat to human health and have become a major medical problem that needs to be urgently addressed [1]. Especially with the rapid spread of multidrug-resistant bacteria (superbugs), the therapeutic effect of traditional antibiotics has been greatly reduced, and new and efficient antibacterial strategies are urgently needed [2]. In this context, metal nanomaterials as an emerging class of biological sterilization materials have received widespread attention from the scientific community due to their unique physical and chemical natures, broad-spectrum antibacterial activity, and potential biosafety. Nanoenzymes as an important branch of metal nanomaterials have

demonstrated strong antibacterial potential by simulating the catalytic function of natural enzymes [3]. They have not only low cost and high stability but also advantages of adjustable catalytic activity, easy large-scale production and storage, providing strong support for the development of new antibacterial therapies [4].

Many scientists have conducted in-depth research on nanoenzymes. Zhao *et al*. developed a carbon-based nanoenzyme antibacterial material using carbon nanotubes and graphene to address the issue of increasing bacterial resistance to antibiotics. This material showed great potential for application in the field of antibacterial technology [5]. Yang *et al*. prepared an arginine nanoenzyme for the treatment of diabetes wounds, which offered a novel approach for treating diabetic wounds by mitigating oxidative stress, enhancing oxygen levels in hypoxic tissues, and facilitating vascular repair among other beneficial effects [6]. Song *et al*. introduced a nanoenzyme to induce initial immunogenic tumor cell ferroptosis in response to the problem of low response rates caused by insufficient tumor cell immunogenicity in existing immunotherapy strategies. The results showed that the nanoenzyme could effectively inhibit and eliminate tumors [7]. Gao *et al*. developed an a-amanitin detection method using carbon dots/gold nanoparticle nanoenzymes (D-Glu-CDs/AuNPs) to address the issue of quickly and effectively detect the a-amanitin toxin in toxic mushrooms. By utilizing glucose carbon dots and sodium citrate as both reducing agents and stabilizers, this nanoenzyme was synthesized and exhibited robust peroxidase-like activity. The results showed that the detection limit of this method was 48.03 ng/mL, indicating high sensitivity [8]. However, there are still many problems in the practical application of nanoenzyme antibacterial and detection such as insufficient catalytic activity, low efficiency of free radical generation, and limited bacterial capture ability, which seriously restrict the further improvement of its therapeutic and detection effects. Therefore, developing nanoenzyme composite materials with high catalytic activity, low toxicity, and strong bacterial binding ability has become an important direction of current research. In recent years, inspired by the phenomenon of bacterial adhesion in nature, scientists have begun to explore the use of nanomaterials with rough surfaces to enhance the capture and killing effects of bacteria. This strategy can not only effectively improve the antibacterial performance of nanomaterials but also overcome their inherent catalytic activity defects to a certain extent. Molybdenum disulfide (MoS_2) nanomaterials, due to their unique peroxidase like activity and biosafety, have become one of the hotspots in the research of new metal nanomaterials. To increase the exposure of catalytic hydrogenation active sites, Huang *et al*. used a simple one-step hydrothermal method and the principle of electrostatic adsorption to self-assemble positively charged MoS_2 nuclei and negatively charged C nuclei layer by layer, constructing MoS_2/C nanomaterials. The results showed that MoS_2/C catalyst exhibited enhanced catalytic performance in the hydrogenation of benzanthracene [9]. Li *et al*. designed an efficient and economically safe antibacterial agent and enhanced its antibacterial effect through CuNPs/MoS_2 composite material. The results showed that, under 660 nm visible light irradiation for 5 minutes, the CuNPs/MoS_2 composite material had excellent antibacterial properties against both Gram-negative bacteria (GN) *Escherichia coli* and Gram-positive bacteria (GP) *Staphylococcus aureus*, killing almost all bacteria [10]. Cai *et al*. designed a novel multifunctional antibacterial system that combined two antibacterial mechanisms of mechanical sterilization (Au-nanostars) and photothermal effect (MoS_2). The targeted molecule vancomycin was modified on the top of MoS_2-Au nanocomposites to enhance their antibacterial performance and targeting ability. The results showed that Van-MoS_2 Au nanocomposite material could completely destroy both GN and GP bacteria after 20 minutes of irradiation with 808 nm near-infrared laser [11]. Drawing from these research findings, it is evident that MoS_2 holds immense promise

for applications in catalysis, energy storage, water treatment, as well as antibacterial domains. However, its single performance often makes it difficult to achieve optimal performance when used alone. Reduced graphene oxide (rGO), on the other hand, can effectively improve the performance of MoS_2 due to its high conductivity, large specific surface area, and excellent mechanical properties. The introduction of rGO can effectively improve the dispersibility of MoS_2, reduce agglomeration, and significantly enhance the exposure of MoS_2 catalytic active sites, which not only improves the efficiency of catalytic reactions but also broadens the application scope of MoS_2 in the field of catalysis. The rough surface and strong adsorption capacity of rGO can provide more attachment points for bacteria, while its excellent conductivity helps accelerate the electron transfer process, significantly enhancing the capture and killing effect on bacteria [12].

For the advancement of global public health, this study synthesized nanocomposites of molybdenum disulfide nanosheet on the surface of reduced graphene oxide (MoS_2/rGO) and developed new effective and safer antibacterial materials through a unique vertical heterojunction structure to effectively capture and kill bacteria. The research would expand the application boundaries of nanomaterials in the biomedical field, promote the in-depth development of antibacterial material research, and provide innovative solutions for solving the global problem of drug-resistant bacterial infections.

Materials and methods

Preparation of MoS_2/rGO nanocomposites

The preparation of the new metal nanocomposite material MoS_2/rGO nanocomposites was divided into two steps. The first step was to use high-purity graphite as the starting material and prepare graphene oxide nanoparticles using an optimized Hummers method variant. Briefly, 1.0 gram of graphite flakes (C) (Sigma Company, Ltd, Victoria, Australia) was mixed with 6.0 grams of potassium permanganate ($KMnO_4$) (Shanghai Adamas Reagent Co., Ltd, Shanghai, China) uniformly in a mixed acid solution of concentrated sulfuric acid and phosphoric acid (v/v ration of 100:10 mL) to gradually oxidize the carbon atoms between the layers of graphene under strong oxidation, forming graphene nanosheets rich in oxygen-containing functional groups. The mixture was then heated at 50°C for 12 hours with stirring. After the reaction was complete, the mixture was cooled naturally to room temperature, and 1.0 mL of 30% hydrogen peroxide (H_2O_2) was slowly added to reduce the remaining oxidant, resulting in a bright yellow dispersion. To remove impurities and incompletely react chemicals from the reaction system, the yellow dispersion was centrifuged for 30 minutes. The graphene precipitate was collected and repeatedly washed with a large amount of deionized water. To completely eliminate residual small molecules and ions, the washed graphene suspension was enclosed within a dialysis bag equipped with a dialysis membrane having a molecular weight cut-off of around 3,000 Da and underwent dialysis treatment for two weeks until the dialysis solution attained clarity and transparency, thereby yielding a highly purified graphene suspension. The graphene suspension was freeze-dried at -60°C for 12 hours to obtain a dry and easily processed graphene nanosheet powder. The second step was to use the high efficiency and uniformity of microwave heating to promote the vertical growth of MoS_2 nanosheets on the surface of rGO based on the preparation of graphene nanosheets and assist in the synthesis of MoS_2/rGO vertical heterojunctions. The graphene suspension was dissolved at a concentration of 1 mg/mL with 170 mg of ammonium tetrathiomolybdate ($(NH_4)_2MoS_4$), and 15 mg of ascorbic acid ($C_6H_8O_6$) together in 25 mL of dimethylformamide solvent (C_3H_7NO) and stirred to form a uniform mixed solution before being transferred to a 35 mL pressurized reaction flask and heated to 200°C with magnetic stirring. The reaction system was then maintained in a microwave synthesis system

for 10 hours. During the microwave heating process, the volatilization of dimethylformamide solvent and chemical reactions at high temperatures jointly promoted the nucleation and growth of molybdenum disulfide nanosheets. Meanwhile, graphene nanosheets served as templates and supports, guiding the growth of molybdenum disulfide nanosheets perpendicular to their surfaces, forming MoS_2/rGO vertical heterostructures. After the reaction was completed, the high-pressure reaction flask was cooled naturally to room temperature and the black reaction product was collected and washed multiple times with deionized water and further processed by filtration and drying at 80°C for 4 hours. A MoS_2/rGO heterostructure with a load of 1% rGO was obtained. Similarly, by changing the addition amount of graphene suspension, MoS_2/rGO heterostructures with different percentages of rGO loading were prepared.

Material characterization and determination methods for MoS_2/rGO nanocomposites

The characterization and observation of MoS_2/rGO heterojunction were conducted using the JEM-2100F field emission transmission electron microscope (TEM) (JEOL Ltd., Tokyo, Japan). Briefly, MoS_2/rGO heterojunction was dispersed in ethanol solvent and sonicated to ensure uniform dispersion before a small amount of dispersed liquid droplets were added onto the ultra-thin carbon film of the copper mesh and air dried naturally. The morphology of the heterojunction of prepared sample was observed [13]. The characterization observation was conducted using the SU8010 ultra-high resolution cold field emission scanning electron microscope (Hitachi, Tokyo, Japan). The MoS_2/rGO heterojunction was fixed on a conductive sample stage and then subjected to surface gold spraying treatment to enhance conductivity. The morphology and surface structure were then observed [14]. In X-ray diffraction (XRD) characterization observation, MoS_2/rGO heterojunction powder was ground into fine particles and uniformly spread on the XRD sample stage. A suitable X-ray source with a scanning range of 5° - 90°2θ angles was set up for XRD scanning using Kratos Axis Nova X-ray photoelectron spectrometer (Shimadzu, Kyoto, Japan). The surfaces of MoS_2/rGO heterojunction samples were cleaned with anhydrous ethanol and measured with a Fourier transform infrared spectroscopy after the anhydrous ethanol evaporated.

***In vitro* sterilization experiment of MoS_2/rGO nanocomposites**

To investigate *in vitro* sterilization efficacy of MoS_2/rGO nanocomposites against GN and GP bacteria, its antibacterial properties, bacterial capture efficiency, morphological changes, and potential impact on biomolecules were evaluated. Wild-type *Escherichia coli* (GN) and *Staphylococcus aureus* (GP) were first cultured on beef extract peptone plates, and then transferred to test tube liquid culture medium. The cultures were shaken at 37°C for 12 hours to reach the logarithmic growth phase of the bacteria before collection of bacteria through centrifugation and washed multiple times with deionized water to obtain purified bacteria at the concentration of 5×10^4 CFU/mL. The *in vitro* sterilization experiment was divided into GN bacteria (A) and GP bacteria (B) two large groups. The two large groups were additionally divided into four experimental subgroups including solely PBS treatment, solely H_2O_2 treatment, exclusively MoS_2/rGO treatment, and both MoS_2/rGO and H_2O_2 treatment. The concentration of MoS_2 in each group was 50 μg/mL, while the concentration of H_2O_2 was 50 μM. After half an hour of processing, the bacterial survival rate was determined using the standard plate counting method below [15].

$$\eta = \frac{C}{C_0} \times 100\% \quad (1)$$

where η was the bacterial survival rate. *C* was the bacterial concentration after treatment. C_0 was the initial concentration. The bacterial capture efficiency was determined by mixing 150 μL of prepared bacterial suspension with 1.5 mL of different materials and then shaking and allowing

the bacteria to fully contact the materials. The supernatant was taken for gradient dilution and inoculated onto trypsin soy agar medium, incubated at 37°C for one day before counting. Bacterial capture efficiency (δ) was calculated as follows [16].

$$\delta=1-\left(\frac{A}{A_0}\times 100\%\right) \quad (2)$$

where A was the final concentration of bacteria. A_0 was the initial concentration. After the reaction, the sample was fixed using 4% paraformaldehyde followed by a gradient dehydration process employing varying concentrations of ethanol. Scanning electron microscopy (SEM) was utilized once again to observe any morphological changes in the bacteria and assess the impact of the material on the bacterial cell structure.

In vivo sterilization experiment of MoS_2/rGO nanocomposites

To assess the sterilization efficacy of the MoS_2/rGO nanocomposite in conjunction with H_2O_2 in a mouse skin wound model infected with *Staphylococcus aureus*, as well as to evaluate *in vivo* toxicity, the study involved 40 mice and randomly allocated animals into four groups with 10 mice in each group for comparative analysis under varying treatments on the back wound site, which included directly subcutaneously injection of 50 µL PBS only, 50 µL H_2O_2 only, 100 µg/mL MoS_2/rGO only, and both MoS_2/rGO and H_2O_2. All animal experimental procedures were approved by the Ethics Committee of the Medical College of Zhejiang University, Hangzhou, Zhejiang, China (Approval No. 2023-zju-med-045). A circular wound was created by having the entire layer of skin removed with surgical scissors at about 2 cm on both sides of the mouse's spine. Each wound was infected with 10 µL of the prepared *Staphylococcus aureus* suspension followed by covering with an elastic bandage. The changes of body weight and wound size were recorded every day after 1 week of continuous treatment. The wound infection was regularly checked by using a disposable sterile swab to roll 3 - 5 circles along the wound surface including exudate or necrotic tissue in a sterile environment and collect samples to avoid contacting the surrounding healthy skin. The swab was then immersed in normal saline containing anticoagulant to shake and elute the cells. The precipitated cells were collected by centrifugation, and cell smears were prepared. After Wright Giemsa staining, the number of white blood cells under 400× high power fields were observed and counted by using optical microscope. All animals were euthanized at the end of the experiment and were dissected immediately. The wound tissues and main organs including heart, liver, spleen, lung, kidney were collected for subsequent histological analysis. The collected organs were first fixed in 10% neutral buffered formalin followed by standard paraffin embedding and sectioning. Histological observation was performed using H&E staining [17, 18].

Statistical analysis

The resulting data were statistically analyzed using SPSS 26.0 software (IBM, Armonk, NY, USA). T-test was employed for comparison of the results obtained from the different experimental treatment groups. The *P* value less than 0.05 was defined as the statistically significant difference.

Results and discussion

Analysis of material characterization of MoS_2/rGO nanocomposites

Through systematic material characterization experiments on MoS_2/rGO nanocomposites, key features such as structure, morphology, chemical composition, and physical properties of the composite material were analyzed in depth, thereby understanding the formation mechanism of the composite material and its sterilization performance advantages. The SEM images of MoS_2/rGO nanocomposites demonstrated that the rGO layer functioned as the substrate, upon which a multitude of MoS_2

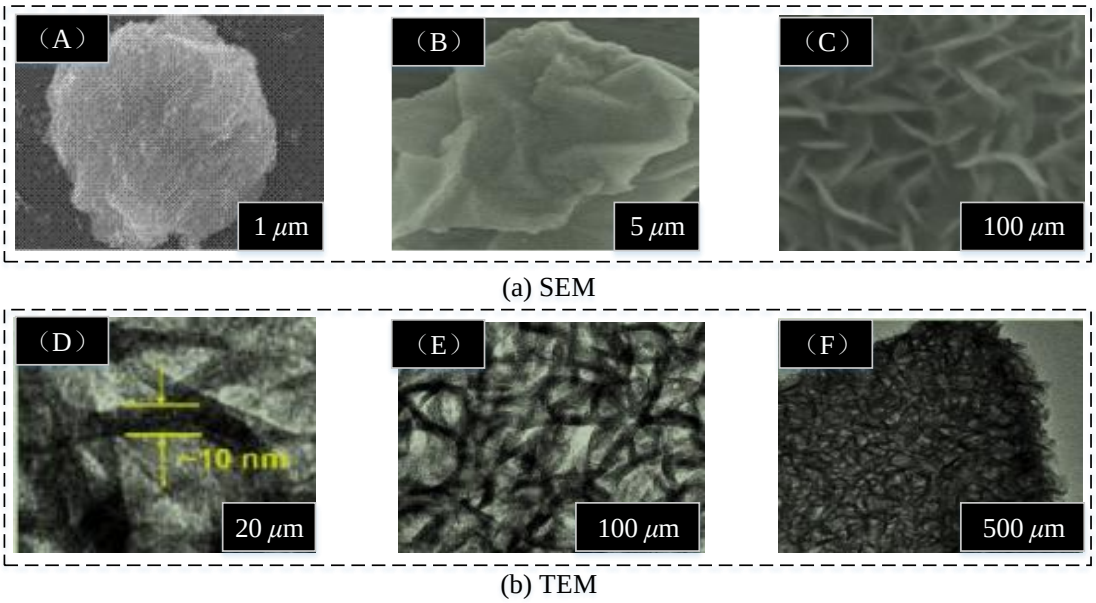

Figure 1. Observation of SEM and TEM images of MoS_2/rGO nanocomposites.

nanosheets were dispersed. The distinct features of the edge morphology, uniform size distribution with an average diameter of approximately 100 nm, and the intimate contact between the MoS_2 nanosheets and the rGO substrate were clearly shown in Figure 1a. On the other hand, the TEM image observations provided insights into the MoS_2/rGO nanocomposites at a different scale, which revealed that the MoS_2/rGO nanocomposites exhibited a characteristic layered structure with interlayer spacings ranging from 6 Å to 70 Å (Figure 1b). The focus of these images was on the edges and defected regions of the MoS_2 nanosheets. Notably, MoS_2/rGO nanocomposites displayed numerous defects, and the crystal stripes along the vertical edges appeared markedly discontinuous. The SEM and TEM image observation results showed that MoS_2 nanosheets were uniformly distributed on the rGO substrate, forming a tightly contacted composite structure. The MoS_2 nanosheets had clear edge shapes and good size consistency. The XRD patterns of MoS_2/rGO nanocomposites showed that the curves of the four test samples had obvious protrusions at 33.5° and 59.1°, which were absorption peaks. The absorption peak at 33.5 ° was on the 100^{th} plane of MoS_2, while the absorption peak at 59.1° was on the 110^{th} plane of MoS_2. However, due to the low mass load of the test sample, the characteristic peak of rGO was not displayed in the image (Figure 2a). The FT-IR spectra of MoS_2/rGO nanocomposites demonstrated that the four tested samples exhibited large and broad peaks in the range of 32×10^2/cm to 36×10^2/cm, which was due to the adsorption of H_2O on the material surface and the stretching vibration of O-H in H_2O. There were small peaks near 28×10^2/cm, 23.6×10^2/cm, and 16.1×10^2/cm, which were due to the bending vibration of MoS_2 (Figure 2b). The XRD pattern and FT-IR spectrum showed the successful composite of MoS_2 and rGO. Further X-ray photoelectron spectroscopy (XPS) was used to investigate the elemental composition and valence of MoS_2/rGO nanocomposites. The XPS spectrum of MoS_2/rGO nanocomposite material 3d orbit of Mo element (Mo 3d) demonstrated two main characteristic peaks located at approximately 227.8 eV and 235.4 eV, respectively, which corresponded to the characteristic peaks of Mo element in the +4-valence state (Mo^{4+}). The presence of Mo^{4+} was a typical feature in the MoS_2 structure, indicating

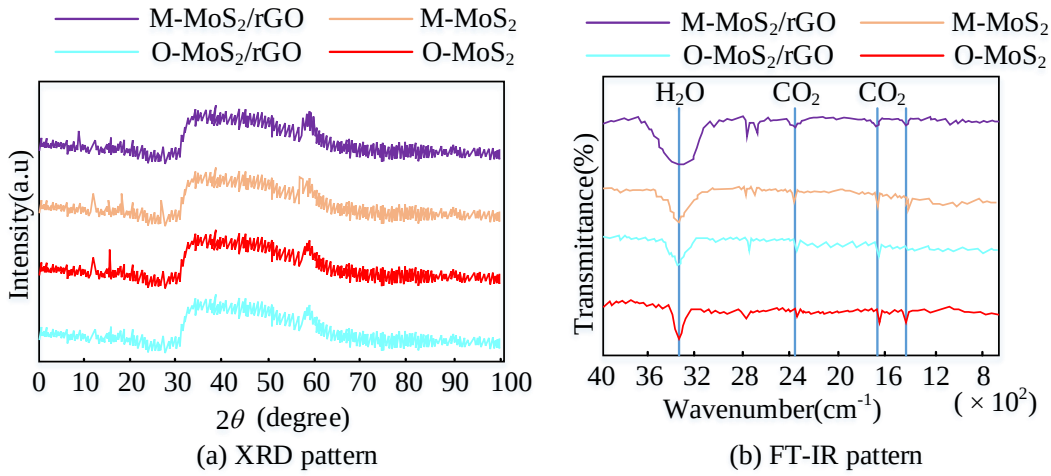

Figure 2. XRD and FT-IR spectra of MoS_2/rGO nanocomposites.

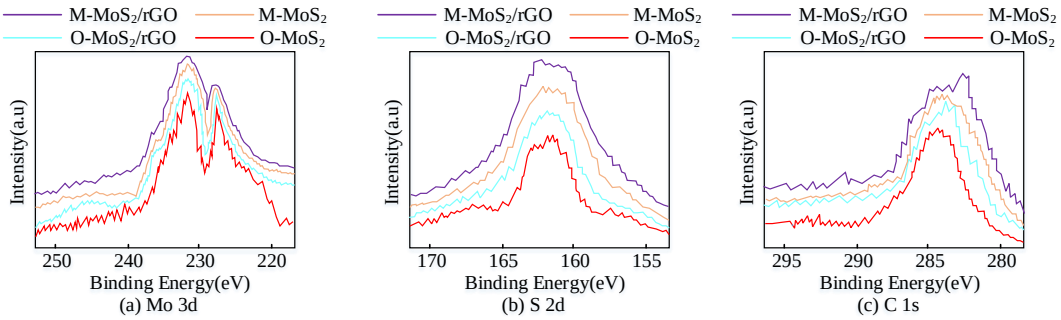

Figure 3. XPS Spectra of MoS_2/rGO nanocomposites.

that Mo atoms formed stable chemical bonds with S atoms. In addition, an S component at 223.12 eV was observed, indicating the presence of defects on the oxide of the composite material (Figure 3a). The 2p orbit of S element (S 2p) spectrum showed that a distinct broad peak was observed from 161.32 eV to 164.35 eV, which corresponded to the characteristic peak of S atoms existing in the MoS_2 lattice in the form of S^{2-} anions (Figure 3b). The existence of S^{2-} was the cornerstone of the formation of the layered structure of MoS_2, and its stable valence state ensured the integrity of the MoS_2 layer and the stability of its electrical properties. The 1s orbit of C element (C 1s) spectrum reflected the chemical state of rGO components in MoS_2/rGO nanocomposites. A major bimodal structure was observed in the spectrum with the peak located at 286.7 eV due to the presence of C-C bonds (Figure 3c). The results indicated that there was an interaction or interface bonding between rGO and MoS_2 in MoS_2/rGO composite materials, which could enhance the overall performance of the composite material. The XPS spectrum displayed the valence states and interactions of Mo, S, and C elements in the composite material, proving the successful synthesis of MoS_2/rGO nanocomposites.

Analysis of *in vitro* sterilization of MoS_2/rGO nanocomposites

The distributions of GN bacterial colonies on the culture medium after different treatments were shown in Figure 4a to 4d, while the distributions of GP bacterial colonies on the culture medium after different treatments were displayed in

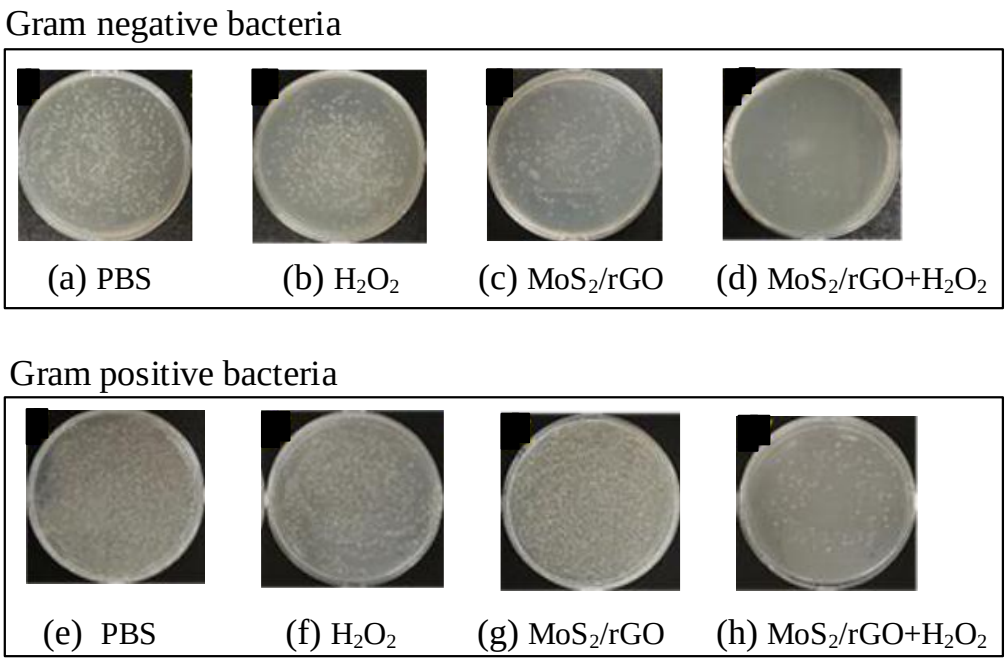

Figure 4. Bacterial colonies after treatment with different materials.

Figure 4e to 4h. Compared to the bacteria treated with PBS and H_2O_2 solutions, the bacterial colonies on the culture medium treated with MoS_2/rGO nanocomposites were significantly reduced. The MoS_2/rGO nanocomposite material had sterilization effects on both GN and GP bacteria. In addition, the culture medium treated with MoS_2/rGO + H_2O_2 showed the fewest bacterial colonies, indicating that the synergistic effect had a stronger sterilization effect. The results of GN bacteria survival rate showed that GN bacteria treated with MoS_2/rGO was about 50%, which was still relatively high. After treatment of MoS_2/rGO + H_2O_2, the bacterial survival rate was about 10%, which was the lowest one (Figure 5a). The results of the GP bacteria survival rate indicated that the bacteria treated with MoS_2/rGO + H_2O_2 also had the lowest survival rate at about 12% (Figure 5b). These results were because H_2O_2 and MoS_2/rGO could have a synergistic effect during the sterilization process. MoS_2/rGO had excellent charge transfer ability and adsorption performance, which could adsorb and fix bacteria, increasing the contact area between bacteria and H_2O_2. Meanwhile, H_2O_2 as a strong oxidant could rapidly penetrate bacterial cell membranes and undergo irreversible reactions, killing bacteria. Therefore, when MoS_2/rGO was used in combination with H_2O_2, the sterilization efficiency could be significantly improved. H_2O_2 could also optimize the surface properties of MoS_2/rGO and improve its antibacterial performance. By adjusting the charge properties and roughness of the MoS_2/rGO surface, the adsorption and capture capabilities for bacteria could be enhanced. In addition, H_2O_2 could also remove pollutants and impurities on the surface of MoS_2/rGO, maintaining its cleanliness and activity, thereby extending its service life and antibacterial effect. The capture efficiencies of different materials for GN and GP bacteria were further tested, and the results showed that the capture efficiencies of different materials for GN and GP bacteria were MoS_2/rGO + H_2O_2 > H_2O_2 > MoS_2/rGO (Figure 6). For GN bacteria, the MoS_2/rGO + H_2O_2 achieved a bacterial capture efficiency of 82.3% in about 40 minutes. It might be because the MoS_2/rGO composite material itself had a large specific surface area and excellent adsorption performance, which could effectively capture bacteria. Although the cell

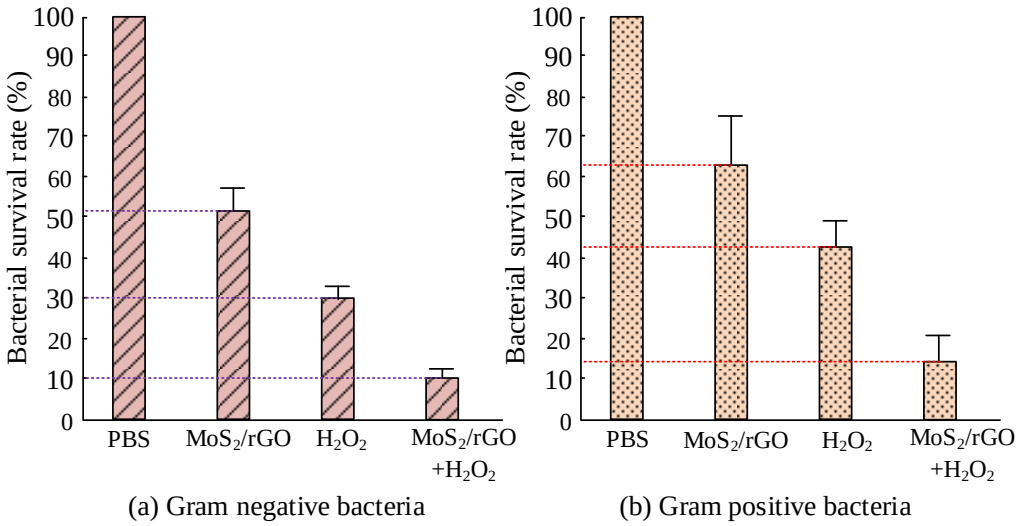

Figure 5. Bacterial survival rates in different treatments.

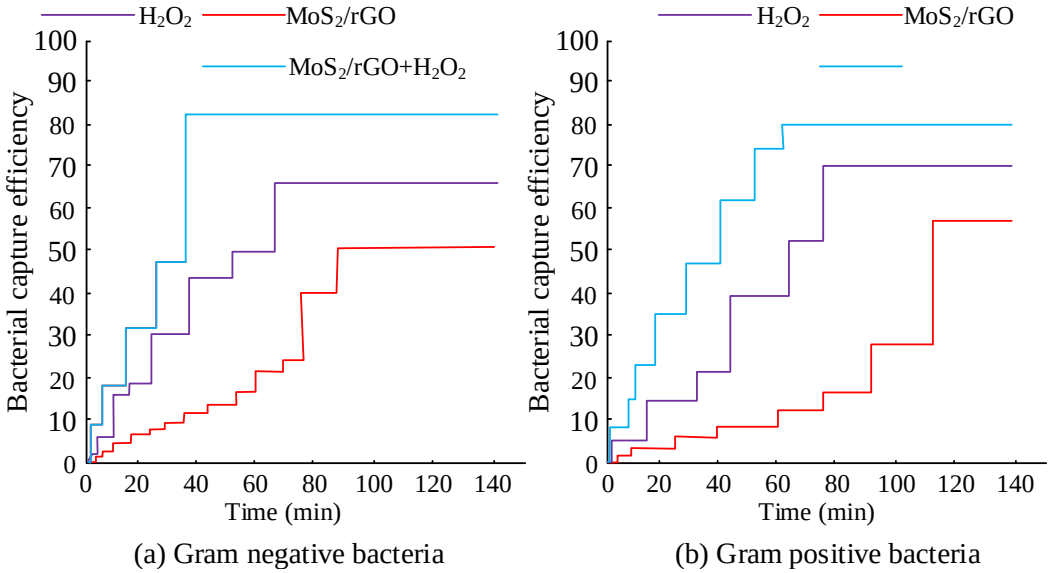

Figure 6. Bacterial capture efficiencies.

wall structure of GP bacteria was different from that of GN bacteria, the MoS_2/rGO + H_2O_2 still achieved a bacterial capture efficiency of 80.3% in about 60 minutes. This result once again confirmed the effectiveness of using MoS_2/rGO composite material in combination with hydrogen peroxide for sterilization.

Analysis of *in vivo* sterilization of MoS_2/rGO nanocomposites

After injecting different materials subcutaneously into the back wounds of mice, the average percentage of wound area and average weight changes of different groups of mice within one week were recorded. Mice in the PBS treatment group were in a state of natural recovery after one week with an average wound area percentage of approximately 76.3%. MoS_2/rGO or H_2O_2 only treatment accelerated the recovery rate of wounds. However, the mice

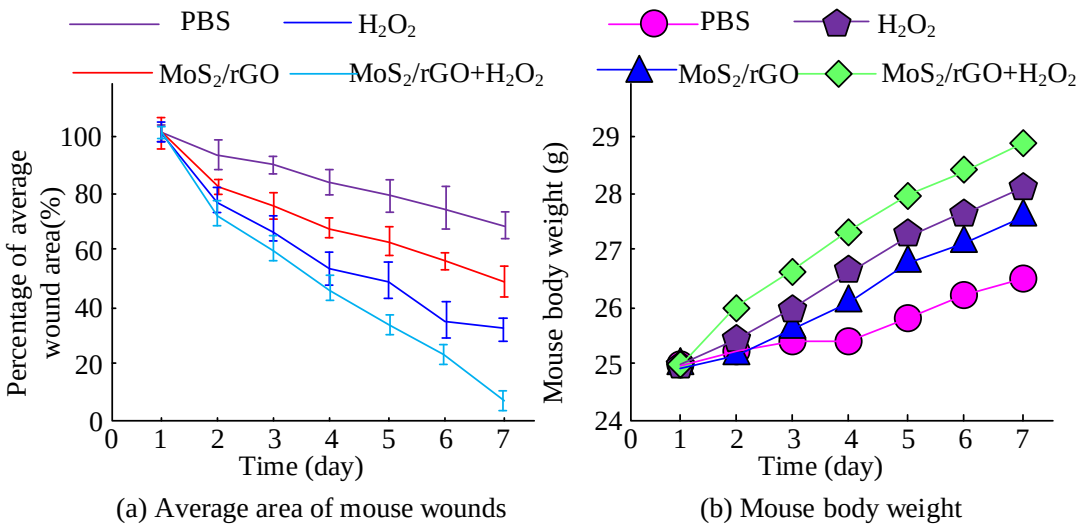

Figure 7. Percentage of average wound area and average body weight of mice.

treated with MoS_2/rGO + H_2O_2 had the fastest wound recovery rate with an average wound area percentage of about 10.2% after one week (Figure 7a). These results might be because the combination of MoS_2 nanosheets and rGO formed a vertical heterostructure, which exposed more edge active sites and enhanced the enzymatic catalytic activity of MoS_2/rGO. These catalytic activities could more effectively catalyze the decomposition of H_2O_2 into reactive oxygen species (ROS), thereby enhancing antibacterial effects and promoting wound healing. The weights of mice injected with MoS_2/rGO + H_2O_2 increased from 25 g to 29 g, showing the largest increase, while the weights of mice in other groups were all below 28 g (Figure 7b), indicating that the health of the mice was generally improved because MoS_2/rGO + H_2O_2 effectively treated the wound, reduced the risk of infection, promoted nutrient absorption, and accelerated the recovery of overall physiological function. After successfully infecting skin wounds with *Staphylococcus aureus* for one day, the wounds were treated with PBS, H_2O_2, MoS_2/rGO, and MoS_2/rGO + H_2O_2, respectively. MoS_2/rGO + H_2O_2 treatment had significant advantages in promoting wound healing and reducing scar formation. On the 7th day, the wounds of the mice were basically healed (Figure 8).

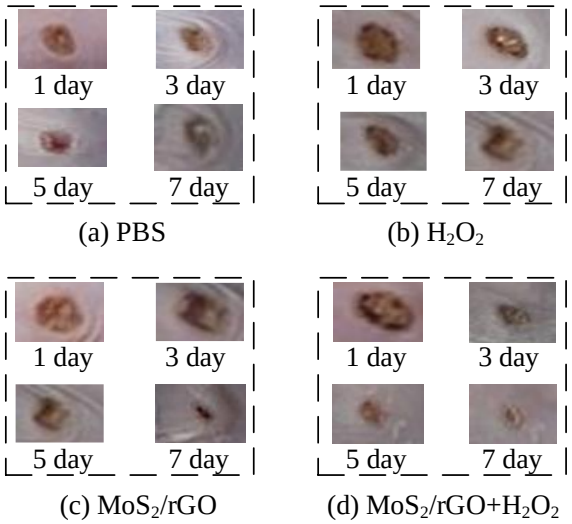

Figure 8. Changes in mouse wounds within one week.

The concentration changes of *Staphylococcus aureus* within one week under four different treatments showed that the MoS_2/rGO and MoS_2/rGO + H_2O_2 treatment groups demonstrated better effects in reducing residual concentrations of *Staphylococcus aureus* (Table 1), which was because MoS_2/rGO had excellent bacterial capture ability and antibacterial effect, and the addition of H_2O_2 might further enhance its bactericidal effect. PBS mainly reduced the bacterial count on the surface of wounds through physical flushing. Therefore, after 7 days, the

Table 1. Changes in *Staphylococcus aureus* concentration in mouse wounds within one week.

Treatment	Day 1 （CFU/mL）	Day 3 （CFU/mL）	Day 5 （CFU/mL）	Day 7 （CFU/mL）
PBS	1×10^6	5×10^5	2×10^5	8×10^4
H_2O_2	8×10^5	2×10^5	5×10^4	1×10^4
MoS_2/rGO	5×10^5	8×10^4	1×10^4	5×10^3
MoS_2/rGO + H_2O_2	3×10^5	5×10^4	5×10^3	< 100

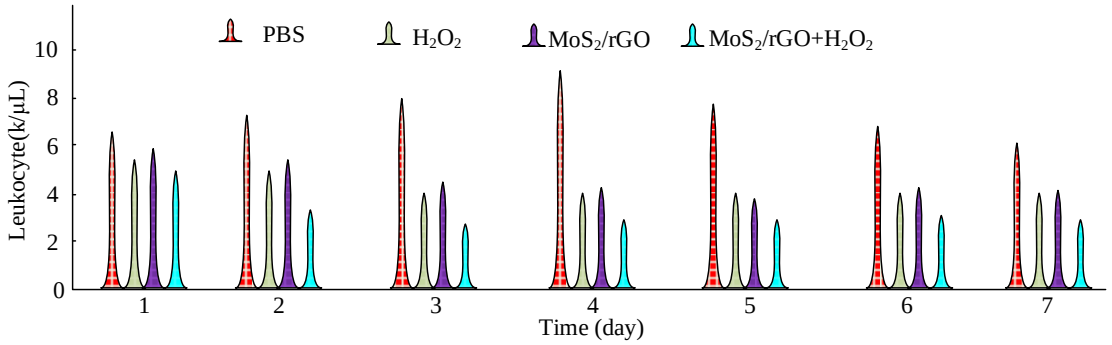

Figure 9. White blood cell count in the wound of different treatments.

residual *Staphylococcus aureus* in the wound was the highest about 8×10^4 CFU/mL. H_2O_2 could penetrate bacterial cell walls and release reactive oxygen species (ROS) inside bacteria such as hydroxyl radicals (OH^-), which could damage proteins, DNA, and lipids inside bacterial cells, leading to bacterial death. In addition, H_2O_2 could also damage bacterial biofilms, further weakening their defense capabilities. After 7 days treatment, there was less residual *Staphylococcus aureus* of approximately 1×10^4 CFU/mL in the wound compared to that of the PBS treatment. The antibacterial mechanism of MoS_2/rGO involved multiple aspects, including that its sharp edges and nanostructures could physically puncture bacterial cell membranes, leading to bacterial death. Both MoS_2 and rGO had excellent charge transfer capabilities, which could adsorb and immobilize bacteria, thereby limiting their movement and reproduction. In addition, MoS_2/rGO might also destroy biomolecules inside bacterial cells by generating ROS, further enhancing its antibacterial effect. The residual amount of *Staphylococcus aureus* in the wound treated by MoS_2/rGO after 7 days was approximately 5×10^3 CFU/mL. The number of white blood cells in the wound of PBS treatment group continued to increase until the 4th day before gradually decreasing, which was because that, in the early stages of injury, the immune system responded quickly and a large number of white blood cells including neutrophils and macrophages were recruited to the wound site to clear pathogens, necrotic tissue, and promote tissue repair. As the wound gradually healed, the inflammatory response weakened, and the number of white blood cells also decreased. The number of white blood cells in the wounds of H_2O_2 treatment group continued to decrease and remained stable at around 3.82K/μL, which was because hydrogen peroxide had antibacterial effects that could quickly kill or inhibit the growth of microorganisms at the wound site, thereby reducing the inflammatory response caused by infection and reducing the demand for white blood cells. The number of white blood cells in the wounds of MoS_2/rGO + H_2O_2 treatment group continued to decrease and remained stable at around 3.51K/μL, which closed to 3.4K/μL in normal mouse, indicating that MoS_2/rGO + H_2O_2 had significant antibacterial activity (Figure 9). MoS_2/rGO nanocomposites served as carriers to

enhance the local concentration and stability of H_2O_2, while their nanostructures might aid in cell adhesion, migration, and proliferation, thereby accelerating wound healing.

Conclusion

The successful synthesis of MoS_2/rGO nanocomposites provided new methods and ideas for the preparation of novel antibacterial materials. The bactericidal effects of MoS_2/rGO nanocomposites *in vitro* and *in vivo* were clarified, especially the synergistic bactericidal effect when combined with H_2O_2, providing theoretical basis and experimental support for the development of efficient antibacterial strategies. This research had potential application value in medicine, food preservation, and other fields. In the future, safety research on MoS_2/rGO nanocomposites will be conducted to evaluate their potential impacts on human health and the environment, ensuring their safety in practical applications.

Acknowledgements

The research was supported by the Young Doctor Research Initiation Fund Project of Harbin University (Grant No. HUDF2023102).

References

1. Hua Z, Fang C, Qiuyu LZ. 2023. Nanoenzyme-reinforced multifunctional scaffold based on Ti_3C_2Tx MXene nanosheets for promoting structure–functional skeletal muscle regeneration *via* electroactivity and microenvironment management. Nano Lett. 23(16):7379-7388.
2. Zhong S, Zhang Z, Zhao Y, Wang S, Hu Q, Li L. 2023. Bismup nanoclusters on nitrogen-doped porous carbon nanoenzyme for cancer therapy. Nanoscale. 15(41):16619-16625.
3. Farooq M, Iqbal T. 2022. Facile hydrothermal synthesis of Cd doped MoS_2 nanomaterials for degradation of organic pollutants: Correlation between experimental and COMSOL simulation. J Inorg Organomet Polym Mater. 32(11):4422-4433.
4. Bat-Ozmatara M, Unlu A, Gevrek TN. 2023. Preparation of isocyanate-containing hydrogel films as antibacterial enzyme immobilization matrices. React Funct Polym. 192(11):1-10.
5. Zhao CX, Gu QM, Chen GY, Yu MB, Liu M. 2021. Research progress of carbon based nanoenzyme and composites in antibacterial field. E3S Web Conf. 267(6):2057-2058.
6. Yang Y, Yang Y, Jiang J, Wu Z, Sun J, Zhi H. 2024. Arginine-nanoenzyme with timely angiogenesis for promoting diabetic wound healing. ACS Appl Mater Interfaces. 16(8):9640-9655.
7. Song X, Liu J, Wang W. 2024. Engineering ternary PdMop nanoenzyme for enzyodynamic effect-enhanced ferroptosis and sonocatalysis-enabled tumor immunotherapy. Adv Funct Mater. 34(10):1-16.
8. Gao J, Peng Z, Song Y. 2024. Colorimetric assay for a-amanitin based on inhibition of carbon dots/AuNPs nanoenzyme activity. Anal Methods-UK. 16(9):1390-1398.
9. Huang R, Yang C, Ta NM, Qu HJ, Wang W, Pan CX, *et al*. 2023. Constructing layer-by-layer self-assembly MoS_2/C nanomaterials by a one-step hydrothermal method for catalytic hydrogenation of phenanthrene. Chem Commun. 59(72):10765-10768.
10. Li J, Ma J, Hong L, Yang C. 2022. Prominent antibacterial effect of sub 5 nm Cu nanoparticles/MoS_2 composite under visible light. Nanotechnology. 33(7):6-10.
11. Cai Y, Wang L, Hu H, Bing W, Zhao J. 2021. A synergistic antibacterial platform: Combining mechanical and photothermal effects based on Van-MoS_2–Au nanocomposites. Nanotechnology. 32(8):85102-85105.
12. Alhammadi A, Alnaqbi W, Rezk A, Nayfeh A. 2021. Using conductive atomic force microscopy to evaluate the electrical properties of MoS_2 nanoparticles for device applications. ECS Transactions. 104(3):17-19.
13. Yang S, Zhang L, Wu Z, Webster RF, Kong C, Chang SLY. 2023. TEM-MD characterization of KDP deformation mechanisms under nanoindentation. J Eur Ceram Soc. 43(8):3844-3848.
14. Mori A. 2022. TEM/STEM-based characterization of aging precipitates in aluminum alloys. J Jpn Inst Light Met. 72(12):717-722.
15. Prada-Ramirez HA, Celeita S, Fonseca JC. 2023. Efficacy comparison of an automated growth-based system and plate-count method on the detection of yeasts and molds in personal care products. J Aoac Int. 106(6): 1564-1573.
16. Voznyak O, Kaplun V, Spodyniuk N. 2023. Efficiency enhancing of the local capture hood due to air barriers. Pollack Periodica. 18(3):58-64.
17. Wu Z, Zhao Y, Zhang N. 2023. A literature survey of green and low-carbon economics using natural experiment approaches in top field journal. Green Low-Carbon Econ. 1(1):2-14.
18. Usman AM, Abdullah MK. 2023. An assessment of building energy consumption characteristics using analytical energy and carbon footprint assessment model. Green Low-Carbon Econ. 1(1):28-40.